

SCIENTIFIC REPORTS

OPEN

Enhancing capacitance behaviour of CoOOH nanostructures using transition metal dopants by ambient oxidation

Yanhui Chen^{1,2}, Junfeng Zhou², Pierce Maguire², Robert O'Connell², Wolfgang Schmitt³, Yonghe Li¹, Zhengguang Yan¹, Yuefei Zhang¹ & Hongzhou Zhang²

Cobalt hydrate and doped binary $\text{Co}_{0.9}\text{M}_{0.1}\text{OOH}$ ($\text{M} = \text{Ni}, \text{Mn}, \text{Fe}$) nanorings of 100–300 nm were fabricated in solution through a facile ambient oxidation method. A transformation from $\text{Co}_{0.9}\text{Ni}_{0.1}(\text{OH})_2$ nanodiscs to hollow $\text{Co}_{0.9}\text{Ni}_{0.1}\text{OOH}$ nanorings was observed with prolonged reaction time. Core-shell nanodiscs have elemental segregation with a $\text{Co}(\text{OH})_2$ core and $\text{Ni}(\text{OH})_2$ shell. $\text{Co}_{0.9}\text{Ni}_{0.1}\text{OOH}$ nanorings displayed a higher electrochemical capacitance than Mn and Fe doped nanorings materials or materials with disc-like geometries.

Hollow inorganic nanomaterials have attracted intense research interest due to low mass density, high porosity and increased surface area^{1–3}. These characteristics make them good candidate materials for high surface area devices such as lithium-ion batteries and gas sensors^{4–8}. Nanorings are one of the hollow structures which have been successfully fabricated and exhibit extraordinary properties due to their ring-like morphology^{9–10}. Divalent metal oxides or their hydrates' nanorings are the most intensively studied hollow materials due to their high surface-to-volume ratio and special magnetic properties^{10–12}. CoOOH is an active material used in conjunction with nickel hydroxide in Ni–H cells. Cobalt oxide is coated on the positive electrodes of rechargeable alkaline nickel batteries to achieve high electrochemical efficiency¹³. In addition, CoOOH is non-stoichiometric and the Co is at a higher oxidation state (+3) than in Co_3O_4 (the oxidation states are +4, +3, +2 and the average is +8/3)^{14,15}. Usually the synthesis process for cobalt/iron hydrates contains a microwave irradiation/ultrasonic chiseling pre-treatment and a high temperature (140 °C–230 °C) post-hydrothermal reaction for few hours^{16–18} with low yield¹⁹. Cobalt hydroxide nanorings have been reported with polycrystalline structure after 10 h in a sealed autoclave at 180 °C²⁰. Hexagonal Co_3O_4 nanorings have also been produced from precursor $\text{Co}(\text{OH})_2$ nanodiscs at 160 °C for 10 h with diameters of a few micrometres¹². Co–Sn–O systems have also been reported using a hydrothermal method at high temperature via the Kirkendall effect through the diffusion of pores²¹. However, other doping such as Mn, or Fe into the $\text{Co}(\text{OH})_2$ is still not reported. A facile room temperature method is needed to prepare doped cobalt hydroxide nanorings with high yield.

Here, we will give detailed preparation and analysis on $\text{Co}_{0.9}\text{Ni}_{0.1}\text{OOH}$ nanorings via ambient oxidation. Typical images of $\text{Co}_{0.9}\text{Ni}_{0.1}\text{OOH}$ products under different reaction times will be discussed, revealing the shape transformation and growth mechanism. Electrochemical properties of CoOOH materials doped with different elements will also be presented.

Results and Discussion

Figure 1 shows the XRD profiles of the products reacted for 3 h (black) and for 72 h (red). The main diffraction peaks in the black spectrum can be attributed to the hexagonal trigonal $\beta\text{-Co}(\text{OH})_2$ structure (JCPDS file No. 30-0443, space group: P3-m1 (166); lattice constants: $a = 3.2 \text{ \AA}$, $c = 4.6 \text{ \AA}$, $\alpha = 90^\circ$, $\beta = 120^\circ$). While weak peaks in the spectrum of 3 h products can be attributed to the $\beta\text{-CoOOH}$ structure (JCPDS file No. 73-1213, space group: Fd-3m (227); lattice constants: $a = 4.7 \text{ \AA}$, $\alpha = 35.5^\circ$). After reaction for 72 h, the peaks of CoOOH were observed

¹Institute of Microstructure and Property of Advanced Materials, Beijing University of Technology, Beijing, 100124, China. ²School of Physics and Centre for Research on Adaptive Nanostructures and Nanodevices (CRANN), Trinity College Dublin, Dublin 2, Republic of Ireland. ³School of Chemistry and Centre for Research on Adaptive Nanostructures and Nanodevices (CRANN), Trinity College Dublin, Dublin 2, Republic of Ireland. Correspondence and requests for materials should be addressed to Y.C. (email: yhchen@bjut.edu.cn)

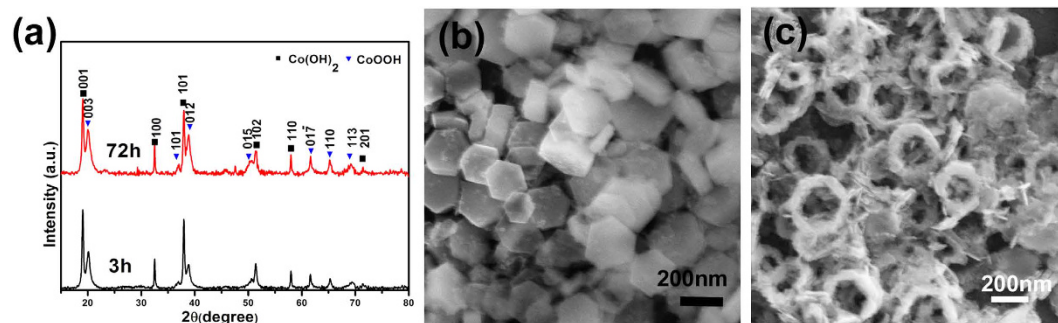


Figure 1. (a) XRD patterns of products after reaction for 3 h and 72 h. Typical SEM image of the synthesized materials for different reaction times for (b) 3 h and (c) 72 h.

to be increased compared to those from $\text{Co}(\text{OH})_2$. This indicates that oxidation continues to occur during this prolonged reaction. Representative SEM images of nanodiscs and nanorings are provided in Fig. 1b,c which displays an outer diameter of 200–300 nm and mean diameter of 230 nm. Statistical SEM results indicate that the yield of nanorings is more than 95% (quantity) in products reacted for 72 h. It can be seen that the surface of the nanorings is rough and composed of loose particles while the inner rings are close to hexagonal shape.

Figure 2 gives typical microstructures of products prepared in 20 °C for 3 h. A typical TEM image in Fig. 1a of a 220 nm outer diameter nanodisc shows that it has uniform thickness. The electron diffraction pattern inset of Fig. 2a indicates its hcp structure with lattice parameters of $a = b = 3.2 \text{ \AA}$ which corresponds to $\beta\text{-Co}(\text{OH})_2$. High resolution transmission electron microscope (HRTEM) images (Fig. 2b,c) from the border and inner space of the nanodisc indicate their single crystal structure. A lattice contraction of about 2% in the $\langle 010 \rangle$ direction of the nanodiscs can be detected, a change from 3.08 Å to 3.02 Å from average measurement results. This contraction can be attributed to the nanomaterials' border effect or structural variation from $\text{Co}(\text{OH})_2$ (lattice parameter a is 3.18 Å) to $\text{Ni}(\text{OH})_2$ (lattice parameter a is 3.11 Å), which has a contraction from about 1.6% to 2.5% in bulk material. The lattice contraction can nearly be omitted in the nanorings, while 1–3 nm amorphous layers can be detected in the outer border of most rings. A further study on the elemental distributions on the room temperature nanodiscs is shown in Fig. 2d–k. It can be seen that the nickel is preferentially distributed in a border range of about 20–30 nm, while the cobalt has a lower concentration in the border compared to the center. The mean concentration of Ni in the border is about 27.5% while it is 6.9% in the center. A schematic illustration of the elemental distribution of the nanodiscs can be observed in the last part of Fig. 2g–k with a $\text{Co}(\text{OH})_2$ core (purplish red color) wrapped by a $\text{Ni}(\text{OH})_2$ shell (azure color).

Figure 3 shows the morphologies, elemental distribution and valence state of nanorings provided from the following techniques: transmission electron microscopy (TEM), energy dispersive X-ray spectroscopy (EDX) and electron energy loss spectroscopy (EELS). In a typical low magnification TEM image in Fig. 3a, tens of rings are shown with diameters from 200–300 nm. Most of the nanorings maintain the hexagonal inner and outer border without any angle variation. The quantitative EDX results show that the ratio of Co/Ni is 87.7/12.3, which contains slightly more Ni than the starting Co/Ni ratio (9/1). A typical EDX map of one nanoring in Fig. 3b shows that the distributions of O, Co and Ni are uniform. An enlarged TEM image in Fig. 3c gives the detailed morphology of the nanorings and shows that the wall thickness of the nanorings is 30–50 nm. Although SEM observations of these nanoparticles suggest a single crystal nanoring, HRTEM results indicate an orientation related multicrystalline structure. The ring-like structure is not comprised of perfect single crystals. The inner edge of the hexagonal border is made of small nanoparticles aggregated continuously or quasi-continuously as in Fig. 3c. A thin porous structure can be seen in the centre of some ring-like structures. A HRTEM image in Fig. 3d indicates that the particles composing the hexagonal skeleton contain a single crystal structure with $\{001\}$ facets of hcp CoOOH as a surface plane. Though the fast Fourier transform (FFT) of the HRTEM in the inset of Fig. 3d gives two sets of the diffraction patterns, the strong spots (indexed by the arrowhead) indicate that the main phase of the product is CoOOH , while it contains traces of the $\text{Co}(\text{OH})_2$ phase. The pre-peak in the EELS spectrum in Fig. 3e of the O edge in 535 eV indicates the existence of OH^- bonds²². Since L_3 and L_2 lines in Co-L edge correspond to transitions from $2p^{3/2}$ to $3d^{3/2}3d^{5/2}$ and from $2p^{1/2}$ to $3d^{3/2}$ respectively, the integration of the L_3/L_2 ratio can provide the ratio of Co^{3+} inside it²³. The L_3/L_2 ratio in the Co-L edge in our rings after calculation is about 2.2 which indicates that the products contain large quantities of trivalent cobalt. From the EELS results, we can conclude that these nanorings are mainly made up of CoOOH .

Figure 4 provides an SEM image of an intermediate state reacted for 24 h and a schematic illustration of shape evolution. In an intermediate state after reaction for 24 h as shown in Fig. 4a, some ring-like structures are formed while most of them maintain a bowl-like structure with a rough surface. The roughness of the surface can be explained by the atomic model in Fig. 4b. In $\text{Co}(\text{OH})_2$ (right part in Fig. 4b) the distance between Co-O layers is 2.66 Å, while it is 2.59 Å in CoOOH (left part in Fig. 4b) due to the loss of H atoms and an electron in the same time. In comparison of the chemical composition of $\text{Co}(\text{OH})_2$ and CoOOH , there is a H-atom removed, which in fact is referring to the removing a proton (H^+ ion) and an electron as well and there forms no $\text{H}(0)$ species. Therefore we say the losing of H atom just in the symbolic meaning to discuss the two atomic models. More surface area in the border is bared to the oxygen-filled environment than in the inner part, resulting in enhanced oxidation of $\text{Co}(\text{OH})_2$ to CoOOH there while the inner part maintains its structure. After reaction for 72 h, ring-like

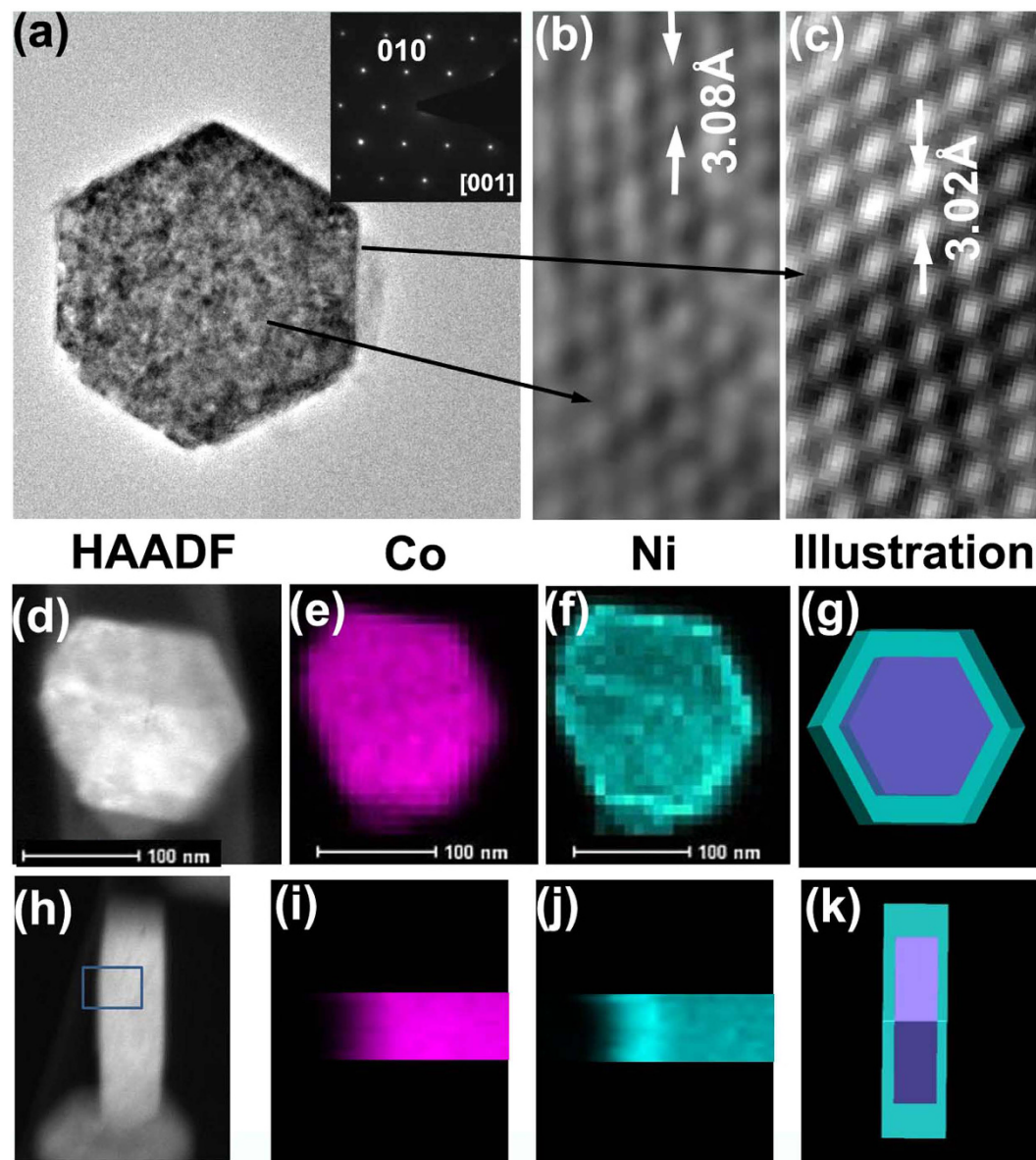


Figure 2. (a) TEM image of a typical nanodisc and its corresponding diffraction pattern. (b,c) HRTEM image on the inner and border of the disc. (d–g) EDX mapping of one top-view nanodisc and its Co and Ni mapping and elemental distribution illustration model. (h–k) EDX mapping of one side-view nanodisc and its Co and Ni mapping and its elemental distribution illustration model.

structures form as shown in Fig. 1c. It indicates the formation of nanorings from the disks which first become porous and finally reach the ring-like structures.

The formation mechanism is illustrated in Fig. 4c. In the beginning, cobalt hydrate precipitates to form a disc-like core and this can be tested by EDX results on samples reacted for short times as shown in Figure S5 and Table S1 in the supplementary information. As time progresses, the loose layered borders and surfaces of β -Co(OH)₂ begin to lose some of their H atoms and an electron due to oxidation. The outer border tends to oxidize to a contracted CoOOH structure since more areas there are exposed to the oxygen. Then a Co(OH)₂/CoOOH boundary will be formed. Inner Co(OH)₂ layers adjacent to the outer CoOOH will then transform/diffuse to CoOOH structure by losing H atoms. Pores will then form in the centre, eventually creating a hollow ring-like structure.

The lowest pH value needed for precipitation can be calculated using the following

$$\text{pH} = 14 - \frac{1}{n} \left(1 \text{ g}[M^{+n}] - 1 \text{ g}K_{\text{sp}} \right)$$

where n is the valence of the metal, M represents activity of ions of the metal and K_{sp} is the solubility product constant. In a dilute solution, the activity of ions (also known as effective concentration) can be expressed as

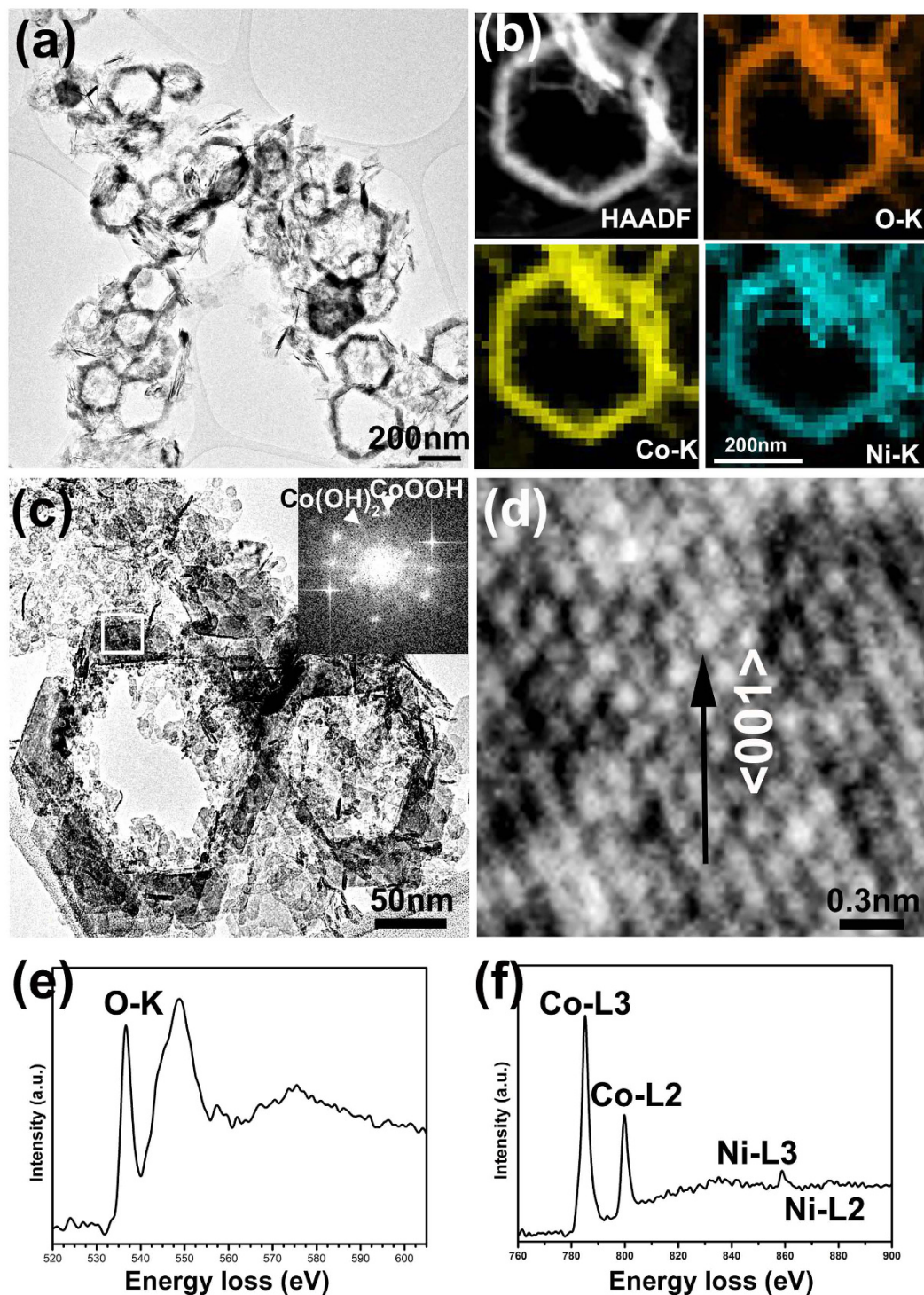


Figure 3. (a) TEM image of hexagonal Ni doped CoOOH nanorings; (b) HAADF STEM image and its corresponding EDX mapping of O, Co and Ni. (c) TEM image and FFT of part of the nanorings and (d) its corresponding lattice image; (e) EELS of O-K edge and (f) Co-L and Ni-L edges.

$a_i = \gamma_i N_i$, where a_i , γ_i and N_i represent of activity, activity coefficient and concentration of the i th ion, respectively. This means that the activity a_i is monotonically dependent on the nominal concentration N_i . Because Co^{2+} and Ni^{2+} have the same valence value, their activities in a dilute solution are very close²⁴. It is reasonable to correlate these thermodynamic quantities with the nominal concentration in this case. Calculation results indicate that if the concentration of Co^{2+} is 0.018 M, the pH value needed is 7.53. Similarly, pH values for a concentration of 0.002 M Ni, Mn and Fe are 7.93, 8.87, and 7.85 respectively. This suggests that the $\text{Co}(\text{OH})_2$ precipitate firstly forms disc-like structures due to its intrinsic hcp structure and provides borders and surfaces to which Ni/Mn/

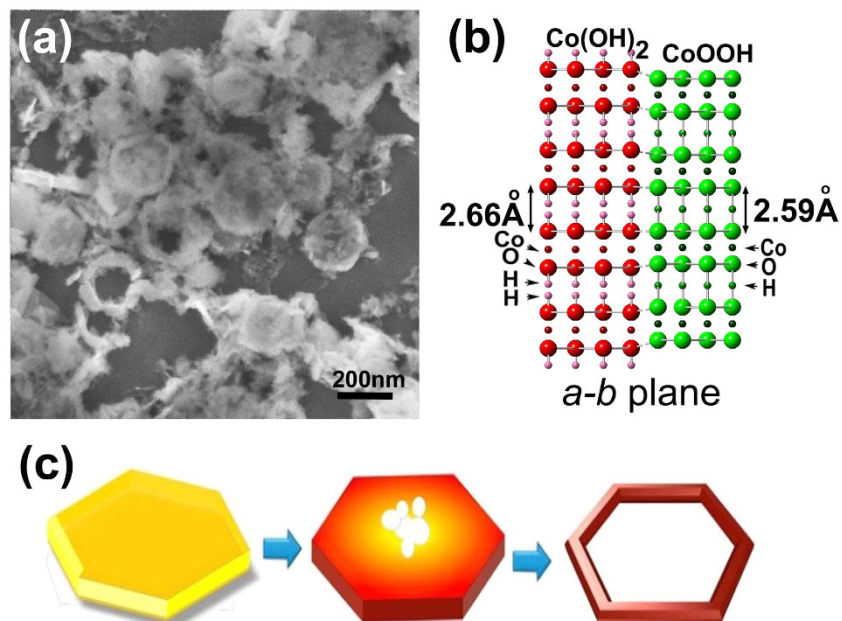


Figure 4. (a) SEM image of typical intermediate products reacted for 24 h. (b) Atomic model of boundary between $\text{Co}(\text{OH})_2$ and CoOOH , in which intervals between layers contract by the loss of hydrogen atoms. (c) The shape evolution is illustrated schematically.

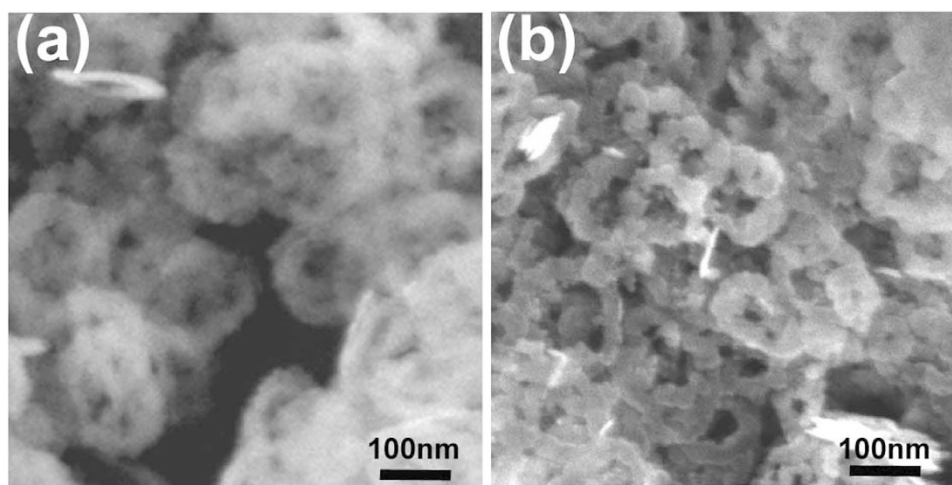


Figure 5. SEM image of typical doped nanorings (a) $\text{Co}_{0.9}\text{Mn}_{0.1}\text{OOH}$ and (b) $\text{Co}_{0.9}\text{Fe}_{0.1}\text{OOH}$.

$\text{Fe}(\text{OH})_2$ can then adhere. That is the reason that no Nickel can be detected in the disc-like structures formed on short timescales while its concentration was found to have increased to 12–3% in ring-like structures (Figure S5 and Table S1). As predicted in the calculation above, Mn^{2+} and Fe^{2+} are possible doping metals with a higher pH value for precipitation needed than Co^{2+} . Typical morphologies and chemical properties of $\text{Co}_{0.9}\text{Mn}_{0.1}\text{OOH}$ and $\text{Co}_{0.9}\text{Fe}_{0.1}\text{OOH}$ nanorings are shown in Fig. 5 and supplementary files (Figure S6–S14). The diameter of $\text{Co}_{0.9}\text{Mn}_{0.1}\text{OOH}$ nanorings is about 150 nm with an average cobalt atomic composition of 91% of metal content. However, the diameter of the $\text{Co}_{0.9}\text{Fe}_{0.1}\text{OOH}$ is about 100 nm with an average cobalt atomic concentration of 89%.

The typical cyclic voltammograms of the $\text{Co}_{0.9}\text{Ni}_{0.1}\text{OOH}$ nanodiscs (black lines) and nanorings were acquired at a sweep rate of 5 mV s^{-1} with a potential window of -0.2 to 0.7 V vs a standard calomel electrode (SCE) and are shown in Fig. 6a and The four peaks of the C-V curve in Fig. 6a can be attribute to transformation of $\text{Co}^{2+} \rightarrow \text{Co}^{3+}$, $\text{Co}^{3+} \rightarrow \text{Co}^{4+}$, $\text{Co}^{4+} \rightarrow \text{Co}^{3+}$ and $\text{Co}^{3+} \rightarrow \text{Co}^{2+25}$. There is a distinct increase in the redox peak of the nanorings compared to that of the nanodiscs. The strong redox peak in the nanorings indicates that the capacitance characteristics are mainly governed by Faradaic reactions, which are very distinct from the rectangular shape of the electric double layer. The charge/discharge curves at current densities of 1 A g^{-1} in Fig. 6b show that after the shape changes to nanorings, its capacitance increased from 211.5 to 439.7 F g^{-1} . The comparison of M doped ($M = \text{Ni}$,

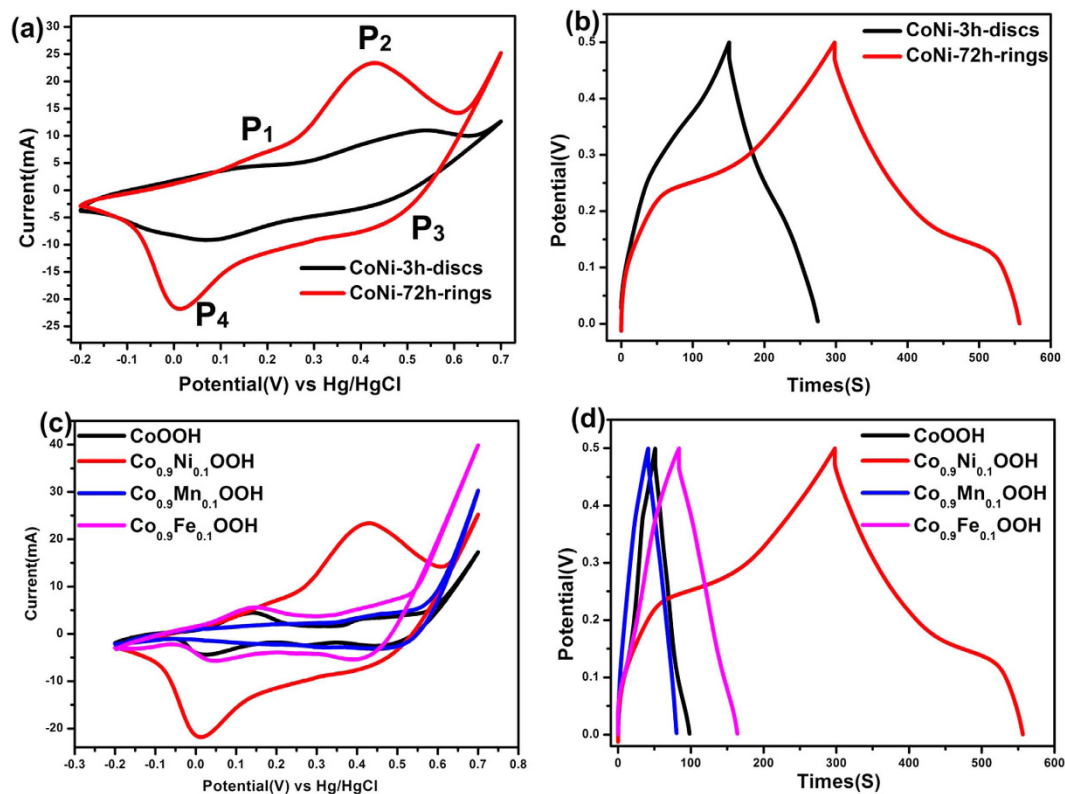


Figure 6. (a) CV curves of $\text{Co}_{0.9}\text{Ni}_{0.1}\text{OOH}$ nanodiscs and nanorings at a sweep rate of 5 mVs^{-1} . (b) Galvanostatic charge/discharge curves of $\text{Co}_{0.9}\text{Ni}_{0.1}\text{OOH}$ nanodiscs and nanorings at discharge current of 1 A g^{-1} . (c) CV curves of M doped $\text{Co}_{0.9}\text{M}_{0.1}\text{OOH}$ ($\text{M} = \text{Ni, Mn, Fe}$) nanorings at a sweep rate of 5 mV s^{-1} . (d) Galvanostatic charge/discharge curves of M doped $\text{Co}_{0.9}\text{M}_{0.1}\text{OOH}$ ($\text{M} = \text{Ni, Mn, Fe}$) nanorings at discharge current of 1 A g^{-1} .

Mn, Fe) nanorings in Fig. 6c,d indicates that Ni doped CoOOH nanorings exhibit better capacitance performance than Mn and Fe doped CoOOH nanorings. The enhanced capacitance can be attributed to the porosity of the surface of the nanorings. We must point out that for pure CoOOH, the nanoring morphology enhances the capacitance but the enhancement is not as significant as the Ni doped ones^{25,26}. This means that both the nanoring morphology and Ni doping can enhance the capacitance.

Conclusions

In conclusion, cobalt hydrate and doped $\text{Co}_{0.9}\text{M}_{0.1}\text{OOH}$ ($\text{M} = \text{Ni, Mn, Fe}$) nanorings were successfully fabricated by shape evolution from $\text{Co}_{0.9}\text{M}_{0.1}(\text{OH})_2$ nanodiscs to $\text{Co}_{0.9}\text{M}_{0.1}\text{OOH}$ nanorings via ambient oxidation in room temperature. The formation and evolution process of the $\text{Co}_{0.9}\text{Ni}_{0.1}\text{OOH}$ system were illustrated. Ring-like structures formed due to the contraction in the surface of the nanodiscs during the oxidation process. $\text{Co}_{0.9}\text{Ni}_{0.1}\text{OOH}$ nanorings displayed a higher capacitance than its disc-like materials and other systems. Nickel doped CoOOH nanorings displayed better capacitance performance than Mn and Fe doped CoOOH nanorings.

Methods

Synthesis of M-doped CoOOH. For the syntheses procedure, Ni doped systems were described as an example, while synthesis with different dopants (Mn, Fe and pure CoOOH materials) use similar methods. In a typical synthesis, $\text{CoCl}_2 \cdot 6\text{H}_2\text{O}$ and $\text{NiCl}_2 \cdot 6\text{H}_2\text{O}$ were dissolved in deionized water with a ratio of 9:1. A small amount of $\text{N}_2\text{H}_4 \cdot \text{H}_2\text{O}$ was added to the solutions. During the reaction, NaOH solution was added to tune the pH value to about 13.7. This solution was continually stirred for 3–72 h in room temperature ($17\text{--}20^\circ\text{C}$) while exposed to the air. A pink brown precipitate in the beginning and then a brown precipitate was collected on the bottom of the bottle. The precipitates were then washed and dried for further characterisation.

Characterisation. An X-ray diffractometer (XRD) on a BRUKER-D8 ADVANCE diffractometer was used while employing a graphite monochromatized $\text{Cu K}\alpha$ radiation flux at a scanning rate of $0.02^\circ \text{ s}^{-1}$ in the 2θ range of 1090° . A Carl Zeiss Ultra scanning electron microscope (SEM) was used to image the morphologies of the Co-Ni hydrate nanoparticles. The SEM was able to perform energy dispersive X-ray spectroscopy (EDX) on the sample. A 300 kV FEI Titan transmission electron microscope (TEM) was also used for imaging and was capable of both electron energy loss spectroscopy (EELS) and EDX. In all cases a wide selection of individual oxide nanoparticles were examined to determine their average structure and morphology.

Electrode preparation and electrochemical tests. Electrochemical measurements were carried out in a 5 M aqueous KOH in a half-cell setup configuration at room temperature. Platinum wire and a standard calomel electrode (SCE) served as counter and reference electrodes, respectively. The working electrode was prepared by casting a paste containing $\text{Co}_{0.9}\text{M}_{0.1}\text{OOH}$ nanomaterials (8 mg), carbon black, and poly(vinylidene fluoride) (PVDF) in a weight ratio of 80:10:10 onto a $1\text{ cm} \times 1\text{ cm}$ Ni foam (2 mm thick, 100 ppi, 95% porosity, purchased from Bitaxiang Co. Ltd., Kunshan, China). The electrodes were calendared and degassed in vacuum at $80\text{ }^\circ\text{C}$ for 12 h. The resulting electrode was pressed at 5 MPa to form about $150\text{ }\mu\text{m}$ thick with $1\text{ cm} \times 1\text{ cm}$ area sheet for electrochemical tests. Cyclic voltammetry (CV) and charge/discharge experiments were obtained on a CHI 660D electrochemistry workstation. CV curves were recorded at a sweep rate of 5 mV s^{-1} with a potential window of -0.2 to 0.7 V vs SCE and cycling performance was investigated at a current density of 1 A g^{-1} .

References

- Caruso, F., Caruso, R. A. & Möhwald, H. Hierarchically Ordered Oxides. *Science* **282**, 1111 (1998).
- Liu, D. *et al.* Co_3O_4 nanocages with highly exposed {110} facets for high-performance lithium storage. *Sci. Rep.* **3**, 2543 (2013).
- Wang, X. *et al.* Cobalt (ii,iii) oxide hollow structures: fabrication, properties and applications. *J. Mater. Chem.* **22**, 23310 (2012).
- Li, W. Y., Xu, L. N. & Chen, J. Co_3O_4 nanomaterials in Lithium-ion batteries and gas sensors. *Adv. Fun. Mater.* **15**, 851 (2005).
- Dames, P. *et al.* Targeted delivery of magnetic aerosol droplets to the lung. *Nat. Nanotechnol.* **2**, 495 (2007).
- Shim, H. S., Shinde, V. R., Kim, H. J., Sung, Y. E. & Kim, W. B. Porous cobalt oxide thin films from low temperature solution phase synthesis for electrochromic electrode. *Thin Solid Films* **516**, 8573 (2008).
- Kartachova, O. *et al.* Evolution of the electrochemical capacitance of transition metal oxynitrides with time: the effect of ageing and passivation. *J. Mater. Chem. A* **2**, 12940 (2014).
- Li, Y. *et al.* Unveiling the dynamic capacitive storage mechanism of Co_3O_4 @ NiCo_2O_4 hybrid nanoelectrodes for supercapacitor applications. *Electrochimica Acta*, **145**, 177 (2014).
- Wu, C. *et al.* Synthesis and Lithium storage properties of Co_3O_4 nanosheet-assembled multishelled hollow spheres. *Adv. Fun. Mater.* **20**, 3666 (2010).
- Ren, S. *et al.* Facile one-pot strategy synthesis of ultrathin α - $\text{Co}(\text{OH})_2$ nanosheets towards high-performance electrochemical capacitors. *Mater. Lett.* **80**, 23 (2012).
- Xing, Z. H., Wang, S. S. & Xu, A. W. Dipole-directed assembly of Fe_3O_4 nanoparticles into nanorings via oriented attachment. *CrystEngComm*. **16**, 1482 (2014).
- Dong, Q., Kumada, N., Yonesaki, Y., Takei, T. & Kinomura, N. Cobalt oxide (Co_3O_4) nanorings prepared from hexagonal β - $\text{Co}(\text{OH})_2$ nanosheets. *Mater. Res. Bull.* **46**, 1156 (2011).
- Hu, W. K., Gao, X. P., Geng, M. M., Gong, Z. X. & Noreus, D. Synthesis of CoOOH Nanorods and Application as Coating Materials of Nickel Hydroxide for High Temperature Ni-MH Cells. *J. Phys. Chem. B* **109**, 5392 (2005).
- Jansson, J., Palmqvist, A. E. C. & Fridell, E. On the catalytic activity of Co_3O_4 in low-temperature CO oxidation. *J. Catal.* **211**, 387 (2002).
- Grillo, F., Natile, M. M. & Glisenti, A. Low-temperature oxidation of carbon monoxide: the influence of water and oxygen on the reactivity of a Co_3O_4 powder surface. *Appl. Phys. B* **48**, 267 (2004).
- Gotić, M., Dražić, G. & Musić, S. Hydrothermal synthesis of α - Fe_2O_3 nanorings with the help of divalent metal cations, Mn^{2+} , Cu^{2+} , Zn^{2+} and Ni^{2+} . *J. Mol. Struct.* **993**, 167 (2011).
- Tao, B., Zhang, Q., Liu, Z. & Geng, B. Cooperative effect of pH value and anions on single-crystalline hexagonal and circular α - Fe_2O_3 nanorings. *Mater. Chem. Phys.* **136**, 604 (2012).
- Ly, B., Xu, Y., Wu, D. & Sun, Y. Single-crystal α - Fe_2O_3 hexagonal nanorings: stepwise influence of different anionic ligands (F- and SCN- anions). *Chem. Comm.* **47**, 967 (2011).
- Zhou, D., Su, X., Boese, M., Wang, R. & Zhang, H. $\text{Ni}(\text{OH})_2$ @ $\text{Co}(\text{OH})_2$ hollow nano-hexagons: Controllable synthesis, facet-selected competitive growth and capacitance property. *Nano Energy* **5**, 52 (2014).
- Chen, Q., Wang, N. & Guo, L. Surfactant-free wet chemical synthesis of $\text{Co}(\text{OH})_2$ nanodisks and nanorings. *Res. Chem. Intermed.* **37**, 421 (2011).
- Peng, C., Gao, L. & Yang, S. Synthesis and magnetic properties of Co-Sn-O nanorings, Chemical Communications. *Chem. Comm.* **42**, 4372 (2007).
- Wirth, R. Water in minerals detectable by electron energy-loss spectroscopy EELS. *Phys. Chem. Miner.* **24**, 561 (1997).
- Wang, Z. L., Yin, J. S. & Jiang, Y. D. EELS analysis of cation valence states and oxygen vacancies in magnetic oxides, *Micron*. *Micron* **31**, 571 (2000).
- Atkins, P. & Paula, J. *Physical chemistry* 8th edn, (ed. Atkins, P. *et al.*) 158–165 (New York, 2006).
- Wang, M., Ren, W., Zhao, Y. & Cui, H. Synthesis of nanostructured CoOOH film with high electrochemical performance for application in supercapacitor. *J. Nanopart. Res.* **16** 2181 (2014).
- Wang, L., Dong, Z. H., Wang, Z. G., Zhang, F. X. & Jin, J. Layered α - $\text{Co}(\text{OH})_2$ nanocones as electrode materials for pseudocapacitors: understanding the effect of interlayer space on electrochemical activity, *Advanced Functional Materials*. **23** 2758–2764 (2013).

Acknowledgements

We would like to thank the staff at the Advanced Microscopy Laboratory (AML), CRANN, Trinity College Dublin. We would like to acknowledge support from the following funding bodies: Science Foundation Ireland [Grants 11/PI/1105, 07/SK/I1220a, 12/TIDA/I2433, and 08/CE/I1432] and the Irish Research Council [Grants EPSPG/2011/239, IRCSET-SolarPrint-2010-02].

Author Contributions

Y.H.C. and J.F.Z. performed experiments and testing. P.M., R.O'C, W.S., Y.L., Z.Y., Y.Z. and H.Z. designed the experiments, discussed the results and co-wrote the manuscript. All authors discussed the results and commented on the manuscript.

Additional Information

Supplementary information accompanies this paper at <http://www.nature.com/srep>

Competing financial interests: The authors declare no competing financial interests.

How to cite this article: Chen, Y. *et al.* Enhancing capacitance behaviour of CoOOH nanostructures using transition metal dopants by ambient oxidation. *Sci. Rep.* **6**, 20704; doi: 10.1038/srep20704 (2016).



This work is licensed under a Creative Commons Attribution 4.0 International License. The images or other third party material in this article are included in the article's Creative Commons license, unless indicated otherwise in the credit line; if the material is not included under the Creative Commons license, users will need to obtain permission from the license holder to reproduce the material. To view a copy of this license, visit <http://creativecommons.org/licenses/by/4.0/>